Multi-resolution remote sensing for flark area detection in boreal aapa mires

Kaapro Keränen, Aleksi Isoaho, Aleksi Räsänen, Jan Hjort, Timo Kumpula, Pasi Korpelainen & Parvez Rana

View supplementary material ⎘

Published online: 24 Jun 2024.

Submit your article to this journal ⎘

View related articles ⎘

View Crossmark data ⎘

Taylor & Francis
Taylor & Francis Group

OPEN ACCESS

Check for updates

Multi-resolution remote sensing for flark area detection in boreal aapa mires

Kaapro Keränen[a,b], Aleksi Isoaho [a,c], Aleksi Räsänen[a,b], Jan Hjort[b], Timo Kumpula [d], Pasi Korpelainen[d] and Parvez Rana[a]

[a]Natural Resources Institute Finland (Luke), Oulu, Finland; [b]Geography Research Unit, University of Oulu, Oulu, Finland; [c]Water, Energy and Environmental Engineering Research Unit, Faculty of Technology, University of Oulu, Oulu, Finland; [d]Department of Geographical and Historical Studies, Faculty of Social Sciences and Business Studies, University of Eastern Finland, Joensuu, Finland

ABSTRACT

Peatlands have suffered significant degradation globally due to human impacts, which has increased the need to monitor the condition and changes in peatland ecosystems. With remote sensing, point-based in-situ observations can be upscaled to larger areas but there is a need to develop scalable monitoring methods. We predicted wet flark area extent, a key ecological indicator for patterned flark fens, in five sites in central Finland. Our primary aim was to test how the spatial and spectral resolution of different optical satellite image products (Landsat 8–9, Sentinel-2, PlanetScope) affect flark area coverage prediction. We also tested if there were seasonal or site-specific differences in prediction accuracy. Lastly, we upscaled the flark area coverage to entire mire areas. We used unmanned aerial vehicle (UAV)-derived flark area classification as a ground reference data to compare satellite sensors' prediction accuracies. We predicted flark area coverage using spectral bands and indices as predictor variables using random forest regression. All sensors provided accurate results with some differences between Landsat (pseudo-R^2 32–84%, root-mean squared error (RMSE) 10 – 18%), Sentinel-2 (R^2 61–92%, RMSE 6 –14%), and PlanetScope (R^2 46 – 92%, RMSE 6 – 17%). The short-wave infrared bands of Landsat and Sentinel-2 did not increase the prediction accuracy. There were notable site-specific variations in prediction accuracy despite all the sites having typical open aapa mire wet flark – dry string patterns. With single-site models, the prediction accuracies were similar for early and late summer data, but when transferring the models to the other sites, performance significantly decreased, especially with the models using the late-summer imagery. Finally, we successfully upscaled the flark area coverage across entire mire areas. Our results demonstrate that the combination of UAV and satellite imagery can be used successfully to monitor peatland conditions and changes in them.

CONTACT Aleksi Isoaho ✉ aleksi.isoaho@luke.fi 🖃 Natural Resources Institute Finland (Luke), Paavo Havaksen tie 3, Oulu 90570, Finland

Supplemental data for this article can be accessed online at https://doi.org/10.1080/01431161.2024.2359732

1. Introduction

Globally, peatlands have degraded because of anthropogenic influence and accelerating global warming (Page and Baird 2016), which has led to the drying of naturally wet ecosystems (Leifeld and Menichetti 2018). As a consequence, the carbon sink and water regulating the functioning of peatland ecosystems has weakened worldwide and many of the peatland habitats and species are threatened (Page and Baird 2016; Strack, Magnus Keith, and Xu 2014; Urák et al. 2017). The changes have been dramatic, especially in the peatland-rich areas within the boreal zone, where 57% the global peatlands are located (United Nations Environment Programme 2022). The degradation has resulted in the need for monitoring changes in the status of the peatlands (Czapiewski and Szumińska 2021; Harris and Bryant 2009). Additionally, Global Biodiversity Framework (2024) suggests that 30% of the degraded peatlands should be under effective restoration by 2030, which further emphasizes the need for cost-effective monitoring methods.

Peatlands have traditionally been monitored with field observations, such as vegetation inventories and water table measurements (Haapalehto et al. 2011; Kolari et al. 2022; Menberu et al. 2016). Additionally, satellite and other remote sensing (RS) techniques have been used in numerous ways in the monitoring (Bechtold et al. 2018; Burdun et al. 2023; Czapiewski and Szumińska 2021; Isoaho et al. 2024; Ozesmi and Bauer 2002; Räsänen, Tolvanen, and Kareksela 2022). For instance, the RS methods are widely applied in the assessment of vegetation cover and composition (Pang et al. 2023; Räsänen and Virtanen 2019; Steenvoorden and Limpens 2023) and wetness (Burdun et al. 2020; Isoaho et al. 2023, 2024; Jussila et al. 2023; Lendzioch et al. 2021; Räsänen, Tolvanen, and Kareksela 2022), which are key indicators for peatland ecosystem functioning. The use of RS methodology is beneficial as in-situ field samplings can disturb the ecosystems and require a lot of laborious field work (Lendzioch et al. 2021). Furthermore, with RS, the point-based field observations can be upscaled to larger spatial extents (Czapiewski and Szumińska 2021; Harris and Bryant 2009; Isoaho et al. 2024).

Optical satellite data has been utilized in peatland research with different spectral wavelengths and spectral indices. Previous studies indicate that optical RS data perform well when modelling peatland surface wetness (Burdun et al. 2020; Isoaho et al. 2023, 2024; Räsänen, Tolvanen, and Kareksela 2022). Typically, utilized indices describe soil moisture conditions, open water cover, and the state of vegetation (Czapiewski and Szumińska 2021; Kolari et al. 2022). However, single bands have outperformed most of the spectral indices in multiple studies targeting soil moisture and water table level (Isoaho et al. 2023; Kolari et al. 2022; Räsänen, Tolvanen, and Kareksela 2022). Nonetheless, the simultaneous use of indices and single bands can provide more comprehensive information for accurately estimating peatland wetness (Isoaho et al. 2024; Räsänen, Tolvanen, and Kareksela 2022).

In addition to satellite RS, high-resolution unmanned aerial vehicles (UAV), also known as drones, have been applied in the RS-based peatland monitoring. UAV images provide accurate and high resolution spatial information, which is needed to correctly classify land cover types in spatially highly heterogeneous peatland ecosystems (Räsänen and Virtanen 2019; Steenvoorden and Limpens 2023; Wolff et al. 2023). UAVs have also been applied e.g. for modelling the spatial patterns of peatlands' water table level (Isoaho et al. 2023), water flow routes, and soil moisture patterns (Ikkala

et al. 2022). UAV can be useful as training data for satellite image applications and for upscaling field-measurements to larger spatial extents (Pang et al. 2023; Räsänen and Virtanen 2019).

While several studies have focused on peatland water table level and soil moisture across the globe (Burdun et al. 2020; Czapiewski and Szumińska 2021; Isoaho et al. 2023; Kalacska et al. 2018; Räsänen, Tolvanen, and Kareksela 2022), less research has concentrated on wet flark area coverage, a key indicator of the ecological condition in northern peatlands (Jussila et al. 2023; Kolari et al. 2022; Tahvanainen 2011; Talvitie, Räsänen, and Silvan 2023). Flark area coverage is an important indicator because it reflects the overall ecohydrological state of flark fens; additionally, flark area has broadly decreased in the boreal aapa mires due to drainage and possibly climate change (Granlund et al. 2022; Kolari and Tahvanainen 2023; Kolari et al. 2022; Sallinen et al. 2019). Even though flarks are semi-permanent microtopographical forms, there are seasonal changes in their spatial extent due variations in peatland hydrology (Talvitie, Räsänen, and Silvan 2023). The site- and season-specific variations in flark coverage also remain mostly unstudied, while site-specific differences have been observed in water table dynamics (Burdun et al. 2023; Räsänen, Tolvanen, and Kareksela 2022).

Multiple studies have compared different satellite sensors and aerial RS methods in modelling of peatlands and wetlands (Bourgeau-Chavez et al. 2017; Burdun et al. 2020; Czapiewski and Szumińska 2021; Kalacska et al. 2018; Klinke et al. 2018; Kolari et al. 2022). Some studies have also compared multiple medium to high spatial resolution satellite imagery to detect land cover and vegetation patterns and open water bodies (Lefebvre et al. 2019; Räsänen et al. 2021; Sirin et al. 2018; Zhou et al. 2017). The respective studies show varying impacts how the spatial resolution affects the predictive capacities of the models, and that higher spatial resolution does not always translate to better prediction performance. However, boreal peatlands have high spatial heterogeneity and it has been discussed that detailed monitoring can be conducted only with fine-resolution UAV imagery (e.g. Ikkala et al. 2022; Isoaho et al. 2023; Steenvoorden and Limpens 2023). Nevertheless, coarser spatial resolution satellite imagery could still be tested in these sites; even though they cannot realistically capture the exact location of peatland microforms, they can potentially be used to assess flark area coverage within pixels and entire peatland complexes.

Satellites provide more autonomous data capture and are temporally more accessible than UAV-based data, which makes them essential to meet the need of cost-effective peatland monitoring. However, different satellite products with varying spatial resolution have not been compared in the prediction of the flark coverage. To address this gap, we utilize RS data from three different resolution optical sensors (Landsat 8–9, Sentinel-2, PlanetScope) to model the flark area coverage of northern aapa mires. We compare the performances of the sensors and develop a method to upscale UAV-based information with satellite imagery. Our specific research questions are the following:

(1) How does the spatial and spectral resolution of different sensors affect the prediction of the flark area coverage?
(2) How does the seasonal and site-specific differences affect the prediction accuracy?
(3) Can the flark area coverage be upscaled to larger peatland complexes?

2. Materials and methods

2.1. Study sites

The research was conducted in five boreal minerotrophic aapa mires: Vihtaneva (26°3′E, 63°52′ N), Haudanneva (26°5′E, 63°49′ N), Kurkineva (26°24′E, 64°6′ N) and Niittysuo (26° 42′E, 65°1′ N) in the Northern Ostrobothnia region, and Vahtisuo (27°35′E, 63°51′ N) in the Northern Savonia region of Finland (Figure 1).

Aapa mires are peat-accumulating boreal peatland complexes that have wet flark fen areas in the middle (Tahvanainen 2011). Flark fen areas consist of water-filled depressions called flarks, and dry hummock called strings; i.e. there is a flark-string pattern (Kolari et al. 2022; Sallinen et al. 2019). The strings are narrow (<10 m) and long (even over 1000 m) elevated micro-topographical forms with vegetation including *Sphagnum* mosses, forbs, graminoids, and some shrubs, while wet flarks are partly covered by shallow (<30 cm), open water with vegetation consisting of *Sphagnum* and wet brown mosses, graminoids and forbs. Flarks are typically wider than but equally long as strings. The edges of the aapa mires are drier consisting of thick peat layers and *Sphagnum*-dominated ground vegetation and are typically sparsely treed pine or spruce mire types (Seppä 2002). The studied areas are mostly treeless open parts of mires, although some Scots pines (*Pinus sylvestris)* and Norway spruces (*Picea abies)* are found in more elevated and drier areas.
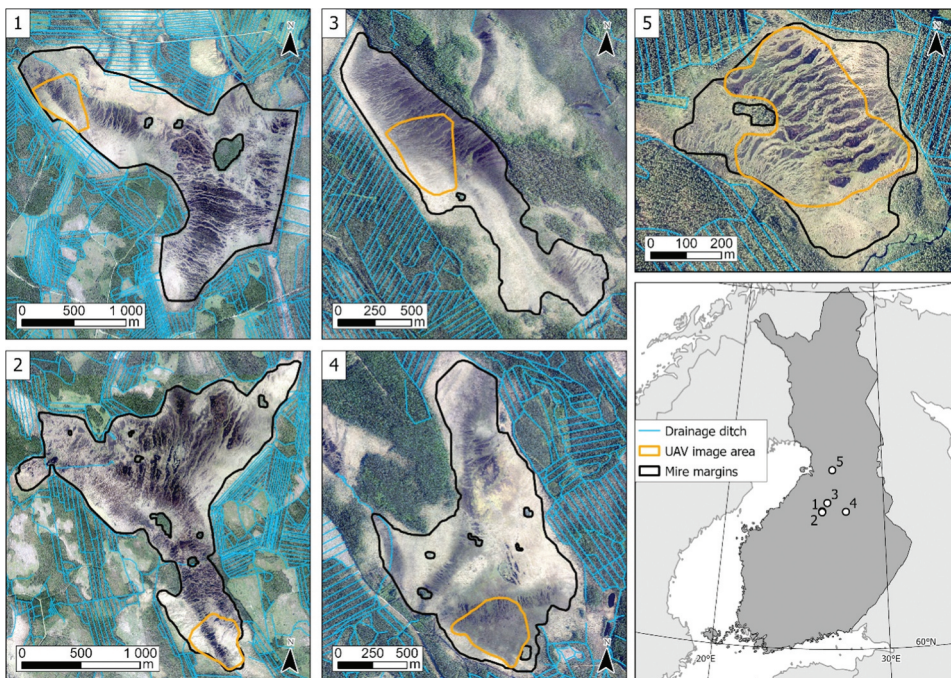

Figure 1. The locations of the study sites: Vihtaneva (1; aerial orthoimage acquired on 27 June 2022), Haudanneva (2; 25 June 2022), Kurkineva (3; 4 June 2021), Vahtisuo (4; 2 June 2021) and Niittysuo (5; 29 June 2021). Delineations within the sites are densely treed areas excluded from the study. Aerial orthoimages are open data from National Land Survey of Finland (2023).

Historically, edges of studied mires were drained for forestry purposes during the 1960s and 1970s. This involved excavating drainage ditches around the mire margins and in the adjacent peatland forest areas. As the aapa mires are dependent on the surrounding surface and near-surface groundwater flows, the drainage led to efficient drying of the mires, including the central unditched areas (Sallinen et al. 2019). Such drying caused the flark ponds to shrink and triggered a shift in vegetation from *Carex*-dominated vegetation to *Sphagnum*-dominated (Granlund et al. 2022; Kolari and Tahvanainen 2023; Kolari et al. 2022; Tahvanainen 2011). More recently, there have been efforts to restore these sites by directing water flow routes from drainage to the unditched but dried parts of the peatland complexes (Isoaho et al. 2023). Ultimately, the restoration processes aim to recover the mire ecosystems to their natural-like state (Haapalehto et al. 2014; Strack, Magnus Keith, and Xu 2014).

While the study sites are similar in terms of drainage and restoration history, there are some notable site-specific differences. Based on Hautala (2022) vegetation inventories and our empirical experiences on the field, Vahtisuo has less *Sphagnum cuspidatum* while having more hummock and forest species coverage indicating less wet conditions than other sites. In the same vein, Niittysuo has more forbs indicating more nutrient-rich conditions than other sites. Kurkineva, Vihtaneva and Haudannaeva are generally similar to each other having a similar coverage of different plant functional groups and flark-string patterns.

2.2. Remote sensing data

We utilized multiple optical RS datasets, consisting of multispectral UAV and satellite imagery (Table 1, Figure 2). We conducted UAV flights with DJI Matrice 300 with real-time kinematic positioning in late May (hereafter early summer) and mid-August (hereafter late summer). Early summer imagery represents the time-point when the water table is typically at its highest right after snowmelt, while late summer represents low water table conditions (Figure S1; Sallinen et al. 2023) in which vegetation cover is close to its seasonal peak (Pang et al. 2023). In Vihtaneva and Kurkineva, we conducted flights in both 2021 and 2022, while at other sites, only in 2021 (Table S1). We collected the data with 5-band MicaSense sensors (RedEdge-M in 2021 and spring 2022, and Altum-PT in August 2022, Table 1) and radiometrically calibrated the imagery with reflectance panels

Table 1. Remote sensing datasets used and their acquisitions dates, bands, spatial resolutions, and sources. UAV refers to unmanned aerial vehicle, NIR to near-infrared and SWIR to shortwave infrared.

| Dataset	Image acquisition date	Captured bands	Spatial resolution	Data source (Reference)
UAV	Early and late summer 2021 & 2022 Early and late summer 2021 & 2022	Blue, Green, Red, NIR, Red Edge	5–10 cm	Authors
PlanetScope	Early and late summer 2021 & 2022	Blue, Green, Red, NIR,	3 m	Planet Labs (Planet Team 2023)
Sentinel-2	Early and late summer 2021 & 2022	Blue, Green, Red, NIR, SWIR1, SWIR2	10 m, 20 m for SWIR bands	European Space Agency (ESA 2023)
Landsat 8–9	Early and late summer 2021 & 2022	Blue, Green, Red, NIR, SWIR1, SWIR2	30 m	U.S. Geological Survey (USGS 2023)
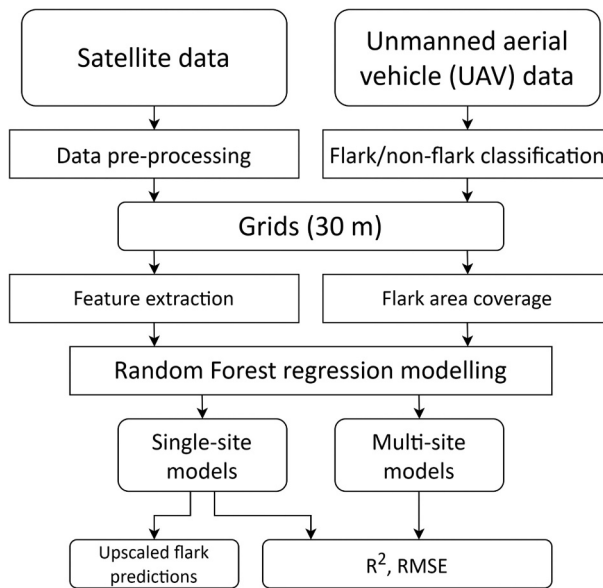
Figure 2. Simplified flowchart of methodology used in this study. R^2: percentage of variance explained and RMSE: root-mean-square error.

and empirical line calibration. The calibrated data were used to construct fine-resolution (5–10 cm) orthomosaics with Agisoft Metashape (version 1.8.4). However, the UAV image of early summer 2021 from Kurkineva was shaded by clouds and therefore, omitted from our analysis. In total, we utilized 13 UAV orthomosaics.

Additionally, we incorporated satellite imagery from three distinct sources: NASA/USGS Landsat 8–9, ESA Copernicus Sentinel-2 and Planet Inc. PlanetScope (Table 1). All satellite data were atmospherically corrected surface reflection products (Level-2 for Landsat, Level-2A for Sentinel, and Planet Surface Reflectance for PlanetScope). We obtained cloud-free satellite data to as close as possible with the UAV flight dates, up to 14 days apart (Table S1). Landsat 8–9 had the lowest temporal frequency between the dates of images, but from late summer, cloudless images were difficult to find also for Sentinel-2 and PlanetScope data.

2.3. Feature extraction

We extracted individual bands and several vegetation and moisture-related indices from the RS datasets (Table 2). We calculated vegetation indices as they have correlated with vegetation greenness and vegetated land cover extent (Kolari et al. 2022; Lendzioch et al. 2021; Riihimäki, Luoto, and Heiskanen 2019; Taddeo, Dronova, and Depsky 2019) and moisture-related indices as they are connected with surface wetness of peatlands and open water cover (Kalacska et al. 2018; Kolari et al. 2022; Meingast et al. 2014). Particularly, we included the Green Difference Vegetation Index (GDVI; Sripada et al. 2006) and Automated Water Extraction Index (AWEI; Feyisa et al. 2014), which have correlated strongly with open water flark areas according to Kolari et al. (2022). Lastly, we added the Enhanced Vegetation Index (EVI; Huete et al. 2002) and Soil Adjusted Vegetation Index

Table 2. List of spectral indices calculated from the Landsat 8–9, Sentinel-2, and PlanetScope data. NIR refers to near-infrared and SWIR to shortwave infrared.

Index	Abbreviation = Equation	Reference
Normalized Difference Vegetation Index	$NDVI = \frac{(NIR-Red)}{(NIR+Red)}$	Rouse et al. (1974)
Normalized Difference Moisture Index*	$NDMI = \frac{(NIR-SWIR1)}{(NIR+SWIR1)}$	Wilson and Sader (2002)
Normalized Difference Water Index	$NDWI = \frac{(Green-NIR)}{(Green+NIR)}$	McFeeters (1996)
Green Difference Vegetation Index	$GDVI = NIR - Green$	Sripada et al. (2006)
Automated Water Extraction Index*	$AWEI = 4 \times (Green - SWIR1) - 0.2 \times NIR + 2.75 \times SWIR2$	Feyisa et al. (2014)
Enhanced Vegetation Index	$EVI = 2.5 \times \frac{(NIR-Red)}{(NIR+6\times Red-7.5\times Blue+1)}$	Huete et al. (2002)
Soil Adjusted Vegetation Index	SAVI = 1.5 X (NIR-RED) / (NIR+RED+0.5)	Huete (1988)

*Only for Landsat and Sentinel.

(SAVI; Huete 1988), as those indices differentiate vegetated and non-vegetated land covers (Poulin, Davranche, and Lefebvre 2010; Taddeo, Dronova, and Depsky 2019). For the extraction process, we constructed 30 m resolution grids based on the pixel dimensions of Landsat images within the study sites. We then calculated the area-weighted mean for each band and index within these grids.

2.4. Flark and non-flark area classification

For the classification of flark and non-flark areas, we utilized Geographic Object-Based Image Analysis (GEOBIA) (Blaschke et al. 2014) segmentation-classification approach on each of the 13 UAV images using ArcGIS Pro. First, we used green, red, and NIR spectral bands from the UAV images in mean-shift segmentation (Comaniciu and Meer 2002) as those bands produced distinctive spatial features based on our initial tests. We set spectral and spatial detail parameters to 19 and 15, respectively, and minimum segmentation size was set to 100 pixels, equivalent to a minimum area of 0.25–1 m^2 per segment. Second, we constructed around 25 training data polygons of both flark and non-flark areas with an average coverage distribution of 27% and 73%, respectively (Table S2). Third, we used the segmented images and training data as input data for random forest classifications (Breiman 2001). We set the maximum number of trees to 200 as typically the performance diminishes, and the model stabilizes after a couple of a hundred trees (Rodriguez-Galiano et al. 2012). To avoid overfitting, we set the max tree depth to 30. Finally, we set the max number of samples to 100,000 since this value erased random noise based on our initial tests. Fourth, we verified the accuracy of the classifications based on 100 randomly generated points and visual interpretation of the UAV images (86–96%, Table S2, Figure S2–S6). Finally, we extracted the percentage of flark area in each 30 m grid cell.

2.5. Regression models for flark area prediction

We used random forest regressions for predicting the flark area coverage in 30 m grids with spectral bands and indices serving as predictor variables and UAV-image

classified flark area coverage being the response variable. Random forest is effective in this context as it can handle multiple predictor variables without being prone to overfitting or multicollinearity (Probst, Wright, and Boulesteix 2019).

First, we developed single-site models, i.e. separate models for each satellite image data for the area covered by one UAV image. We built the models separately for early summer and late summer seasons. For Landsat and Sentinel, we constructed the models both with and without SWIR bands to get comparable results with PlanetScope data which lacked SWIR-bands, and to assess if SWIR-bands were important for the model performance.

Second, to evaluate the transferability of our models across different sites, we combined multi-site datasets for each sensor, separately. We split the data into training and test sets so that the data from four sites were used as training data and the fifth site was the testing data. We repeated the model so that all sites were used once as testing site and constructed the models both with-SWIR and non-SWIR datasets, and for early summer and late summer seasons.

We opted for the default parameter setting: 500 trees and one-third of variables tried at each split, as default values have been found to be sufficient when using RS data (Belgiu and Drăguţ 2016; Probst, Wright, and Boulesteix 2019). We assessed the model performance based on the percentage variance explained (random forest pseudo-R^2) and root-mean-square error (RMSE). For single-site models, we utilized a 10-fold cross-validation, and for multi-sites, we assessed the performance with the test sites' fit. We also extracted variable importance for the models utilizing percentage increase in mean square error statistic. We summed the importance of the predictor variables and normalized the values between 0 and 100 for each sensor and model type (i.e. sensor-specific single-site and multi-site models of with-SWIR and non-SWIR datasets). We conducted the modelling and cross-validation with the *caret* package (Kuhn 2008) in R (version 4.3.0).

Finally, we upscaled the model predictions to 30 m Landsat grids (see section 2.3) covering the entire aapa mires and compared the predicted flark area maps to visual interpretation of aerial orthoimagery (50 cm pixel size, National Land Survey of Finland). For upscaling, we selected the single-site model with the generally best-performing season for each site. If with-SWIR models performed better than non-SWIR models, these were used in the case of Sentinel-2 and Landsat models. We upscaled each sensor type separately to evaluate whether there were noticeable differences among the used satellite datasets.

3. Results

3.1. Different sensors for flark area prediction

In the single-site models, median R^2 values were high (84–92%) and RMSE values (6–10%) relatively low for all sensors (Table 3, Figure 3). On average, the models based on Landsat had lower predictive capacity compared to Sentinel-2 and PlanetScope-based models, the latter two having very similar performances. The exclusion of SWIR data

Table 3. Regression models accuracies by each sensor, single-site and multi-site models with SWIR and non-SWIR datasets. Models' performances are portrayed by median values of variance explained % (R^2) and root-mean-square error (RMSE) values of predicted flark percentage (%).

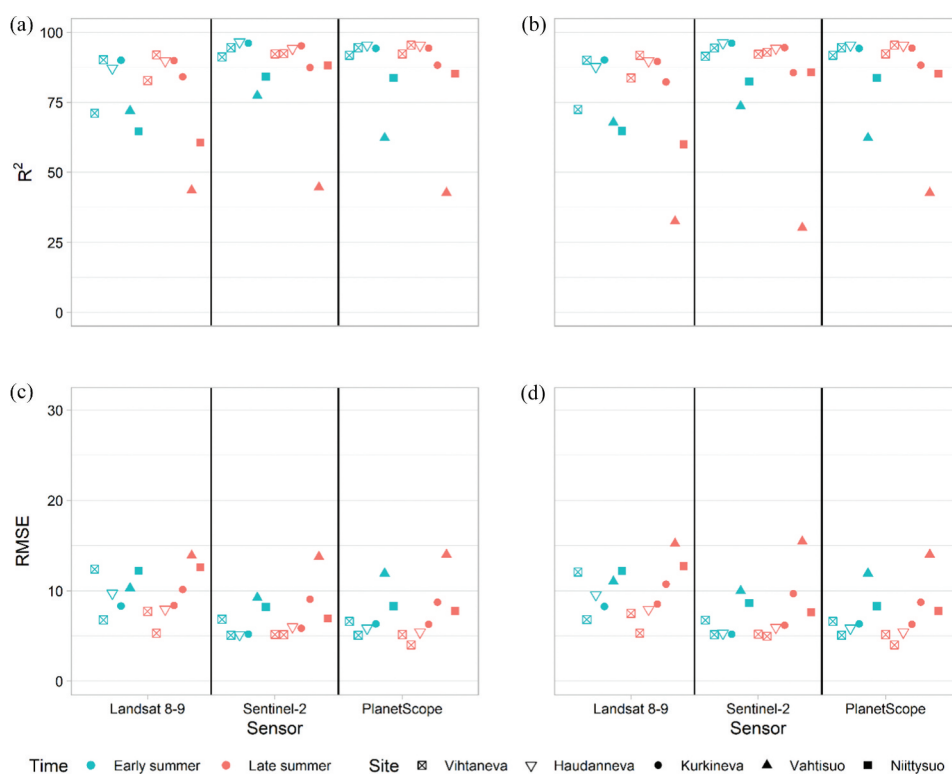|	Single-site				Multi-site			
	With-SWIR		Non-SWIR		With-SWIR		Non-SWIR	
Sensor	R^2 (%)	RMSE (%)	R^2 (%)	RMSE (%)	R^2 (%)	RMSE (%)	R^2 (%)	RMSE (%)
Landsat 8–9	84.1	9.7	83.7	9.6	33.1	17.6	31.7	17.5
Sentinel-2	92.3	6.0	92.2	6.2	61.4	13.1	61.0	13.6
PlanetScope			92.3	6.3			45.9	16.8

Figure 3. Single-site Random Forest regression models results. The variance explained % (R^2), (A, B), and root-mean-square error (RMSE) of the flark area coverage predicted (%), (C, D). The sub-figures a and C represent the models with SWIR datasets and sub-figures B and D with non-SWIR datasets. For PlanetScope, the same results are replicated for both types of models.

did not remarkably change the model performance for Landsat and Sentinel-2 data (Table 3).

Multi-site models had notably lower performances than the single-site models, with more variation in the accuracies between models based on different sensor data (Figure 4, Table 3). While Sentinel-2-based multi-site models' performances stayed relatively high, the performance of Landsat and PlanetScope models decreased
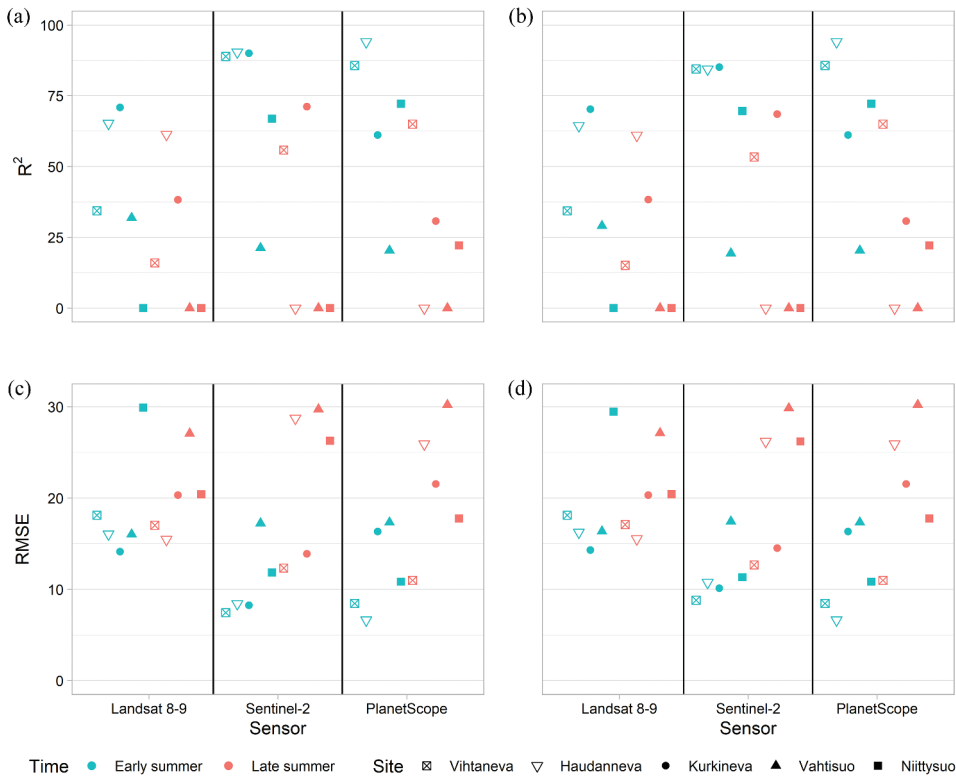
Figure 4. Multi-site Random Forest regression models results. The variance explained % (R^2), (A, B), and root-mean-square error (RMSE) of the flark area coverage predicted (%), (C, D). The subfigures a and C represent the models with SWIR datasets and subfigures B and D with the non-SWIR datasets. For PlanetScope, the same results are replicated for both types of models. Negative R^2 are shown as a 0.

remarkably (Table 3). The performance of multi-site models did not drastically vary between SWIR and non-SWIR datasets.

An analysis of variable importance across all datasets revealed consistent trends (Figure 5). The most important variables were consistently the NIR, green and red bands, and GDVI. In contrast, the SWIR bands and indices that utilized SWIR data had low importance in the models.

3.2. Seasonal and site-specific differences

In the single-site models, Vihtaneva, Haudanneva and Kurkineva had the highest performance, with R^2 values between 71.1 and 96.5%. In contrast, Vahtisuo models showed the poorest performance ($R^2 = 30.2–77.4\%$; Figure 3). Notably, in the single-site models, the overall difference between seasons was negligible, except for a notable deviation in Vahtisuo during late summer.

Multi-site models displayed greater variability among sites and seasons, along with more pronounced differences between the highest and lowest values of model
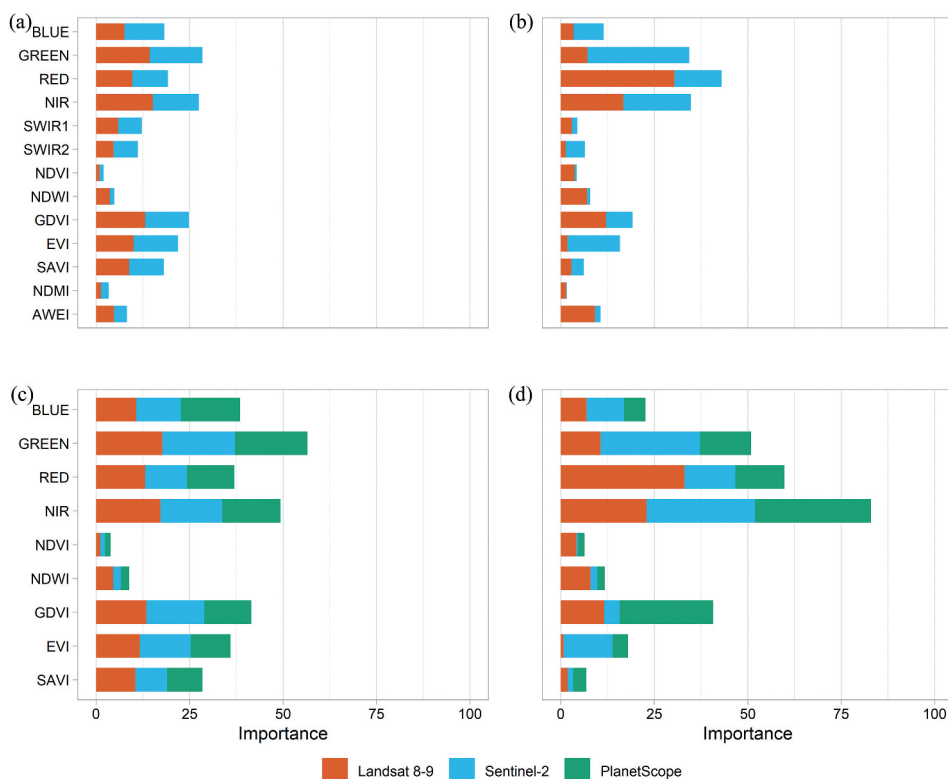
Figure 5. Spectral variable importance is shown as the percentage increase in mean square error. Figures (A, C) represent the single-site models and (B, D) multi-site models. Figures (A, B) represent the models with-SWIR datasets and (C, D) non-SWIR datasets. Variables and index acronyms are explained in Table 2.

accuracies (Figure 4). The ranking of sites in term of performance remained consistent, with Vahtisuo and Niittysuo at the lower end, with some models even having negative R^2 values. There were clear differences between seasons since models of early summer had notably better performance than late summer.

3.3. Upscaling to larger areas

When upscaling model predictions to larger areas, Sentinel-2 and PlanetScope models predicted the spatial flark-string patterns more realistically than Landsat models (Figure 6). This was particularly evident when the predicted maps are visually compared with the flark-string pattern in aerial orthoimagery (see Figure 1). The most notable examples of this were observed in Vihtaneva and Haudanneva, where the flark area patterns depicted in the Sentinel-2 and PlanetScope model-based maps were quite distinct, while in the Landsat-models the strings between flarks are not similarly distinguishable due to smoother prediction outcome. Despite these differences, the predicted values between the sensors were generally close to each
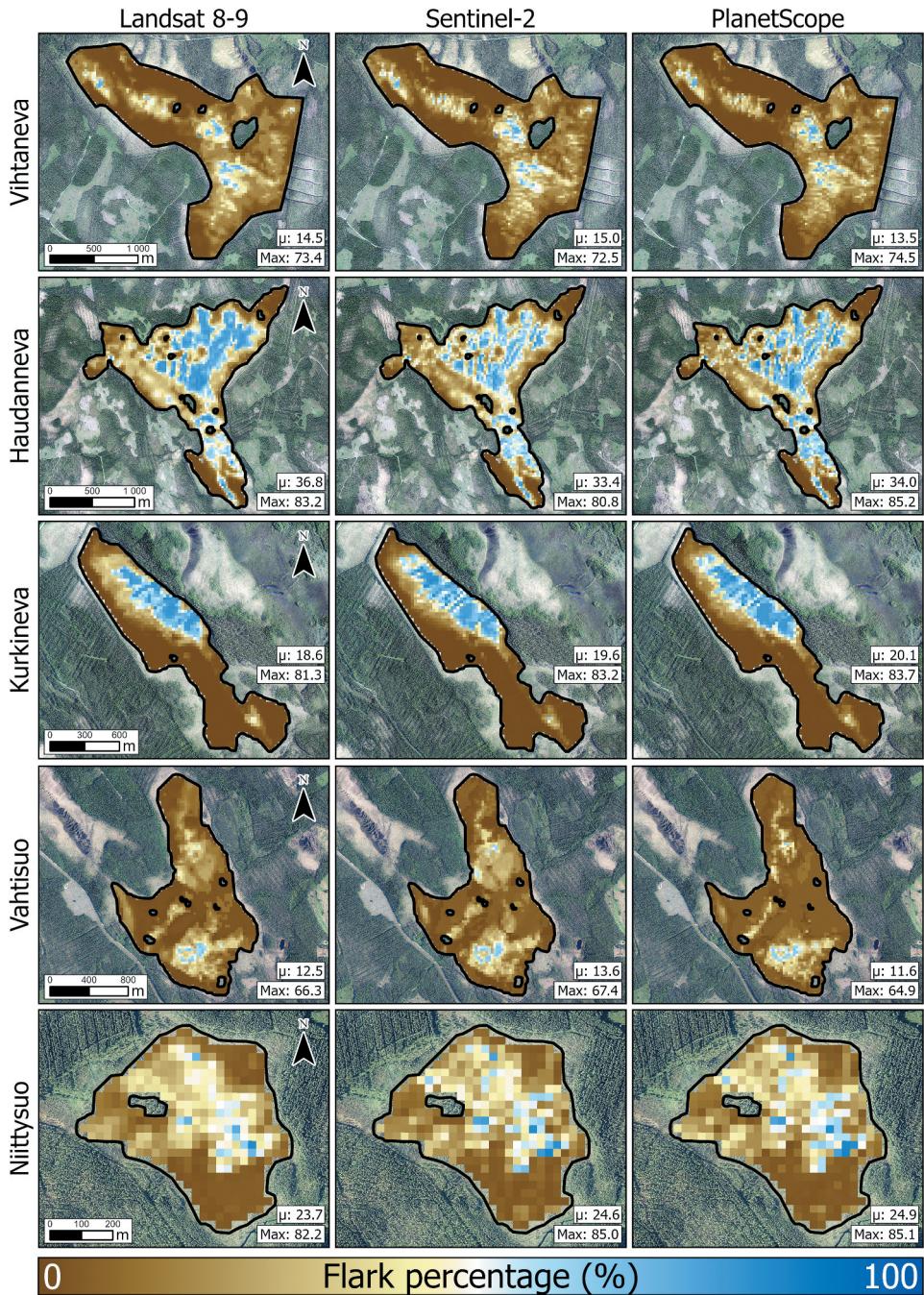
Figure 6. Models' predictions upscaled to larger areas. Predicted area is delineated with black line, masking out mire margins and densely treed areas inside mires. The dates of the models were from late summer 2022 for Vihtaneva, late summer 2021 for Haudanneva, early summer 2022 for Kurkineva, early summer 2021 for Vahtisuo and late summer 2021 for Niittysuo. The mean (μ) and maximum (Max) values of grid flark % are shown for each mire's prediction. Aerial orthoimagery in the background are open data (National Land Survey of Finland 2023).

other, with the landscape-level mean flark coverage differing only by a few percentage points.

4. Discussion

Our study demonstrates that flark area coverage can be accurately predicted using a combination of UAV-based flark area classification and regression models that utilize medium to high spatial resolution (3–30 m) optical satellite imagery. However, there are some differences between satellite image sensors, sites, and seasons in the model performance.

4.1. Spatial and spectral resolution effects

The effect of spatial resolution was to some extent evident as finer resolution imagery of Sentinel-2 (10 m) and PlanetScope (3 m) generally provided better model performance than the coarser resolution Landsat models (30 m). However, the performance of Sentinel-2 and PlanetScope was almost similar. This observation is contradicted by earlier studies that have suggested the use of very high resolution imagery in patterned peatlands (Räsänen and Virtanen 2019; Steenvoorden and Limpens 2023) but aligns with Räsänen et al. (2021), who found no significant advantage of PlanetScope over Sentinel-2 in modelling aboveground biomass patterns in northern peatlands and Arctic tundra. The finding can be related to the lower radiometric quality of PlanetScope when compared to Sentinel-2 (Frazier and Hemingway 2021), which might limit its predictive capacity despite its high spatial resolution.

While we found that Landsat models had the worst performance, the overall difference between the tested sensors was modest because on a landscape level, the difference between overall flark coverage varied only by a few percentage points. Additionally, in single-site models, the performance between sensors was mostly very close to each other (Figure 3). This observation is consistent with Lefebvre et al. (2019), who found that Sentinel-2 did not significantly improve in landcover classification over Landsat imagery. Similar findings were drawn by Sirin et al. (2018), where higher spatial resolution (6 m) did not enhance prediction accuracy compared to Landsat 8 or Sentinel-2. These modest differences imply that datasets of different sensors could be fused to construct dense time-series to monitor changes in peatlands as suggested by (Räsänen, Tolvanen, and Kareksela 2022). However, in the multi-site models, the differences between the sensors were larger than in the single-site models, and there was also more variation between sites.

In our results, the predictive performance for the datasets with and without SWIR bands were similar. This contrasts with earlier studies that have highlighted the importance of SWIR data in the modelling of peatlands' flark area (Jussila et al. 2023) and moisture and water table level (Burdun et al. 2020; Kalacska et al. 2018; Räsänen, Tolvanen, and Kareksela 2022). Instead, our results indicated that green, red, and NIR bands were the most important predictor variables. The lack of importance of SWIR might be related to the fact that we did not model water table or soil moisture, but instead, used flark area extent as our indicator for the hydrological and ecological status of peatlands. Kolari et al.

(2022) had a similar approach and a similar result: SWIR bands did not correlate as strongly as NIR bands with the flark area. However, a relatively high correlation between the peatland water table and individual NIR bands was also demonstrated by Isoaho et al. (2023). We also found out the vegetation indices such as GDVI, EVI, and SAVI were among the most important and outperformed the tested wetness indices. A possible avenue for future studies could be utilizing other NIR or SWIR-based trapezoid models such as OPTRAM (Sadeghi et al. 2017) or its newer variant (Sadeghi et al. 2023) OPTRAM has consistently correlated with the peatland water table, outperforming several wetness and vegetation indices as well as individual bands (Burdun et al. 2023; Räsänen, Tolvanen, and Kareksela 2022).

4.2. Site-specific and seasonal variability

Our results indicate differences in model performance among sites. However, the models for the three best modelled sites (Vihtaneva, Haudanneva, Kurkineva) had relatively similar performance. All these sites have similar flark-string patterns in the centre with drier *Sphagnum* and shrub-dominated areas surrounding them. Niittysuo, a site with moderate model results, has also distinct patterns with large flarks but no dry margins at all. The least accurate models were produced for Vahtisuo, which had a more unclear and scattered flark-string patterns than the other sites. This characteristic possibly makes it difficult to distinguish between flark and non-flark surfaces with the satellite imagery. Additionally, the entire area surveyed by UAV in Vahtisuo underwent significant seasonal changes, being covered by shallow open water in early summer but with no open water coverage in late summer (Figure S5), which possibly hampered the modelling for this site in late summer. Other studies regarding peatland wetness have also identified that relatively similar sites can have different modelling performances caused by small site-specific differences such as historical development of the site or tree coverage (Klinke et al. 2018; Räsänen, Tolvanen, and Kareksela 2022).

Based on our results, single-site models performed the best while multi-site models had lower performance and more variability. Therefore, the approach of training models with data from multiple sites and testing them on a single site seems to lead to inferior performance than training and validating a model in one site due to site-specific differences (Belgiu and Drăguţ 2016; Juel et al. 2015; Räsänen, Tolvanen, and Kareksela 2022; Vetrivel et al. 2015). This implies underlying site-specific variation which have been discussed in (Burdun et al. 2023; Klinke et al. 2018; Räsänen, Tolvanen, and Kareksela 2022). In our results, the multi-site models performed worse in Vahtisuo and Niittysuo than in the other sites, which could be due to differences in ground vegetation. Kurkineva, Vihtaneva and Haudanneva were relatively similar to each other, while Niittysuo and Vahtisuo had more unique ground vegetation patterns (Hautala 2022). Still, the transferability of the models seemed to be possible for some sites, but a larger sample size with more variation in on-site conditions is required for more robust evidence on transferability.

The seasonal differences in single-site models were small, except for Vahtisuo. However, in multi-site models, there was greater seasonal variation, with late summer models performing less accurately than early summer models. This is likely due to the imagery from this period featuring clearer distinctions between water and non-water

covers, a result of a higher water table (Menberu et al. 2016; Sallinen et al. 2023) and reduced vegetation cover (Pang et al. 2023). Nonetheless, some models for early summer underperformed, possibly due to temporal gaps (over 10 days; Table S1) between UAV and used satellite images which might be representing different phenological and hydrological conditions. Earlier, Cole et al. (2014) have highlighted that peatland vegetation is spectrally the most separable during early or mid-growing season but suggested that the optimal temporal window for RS data collection is dependent on the study question.

4.3. *Upscaling and model application*

Despite the challenges with multi-site transferability, the upscaling of single-site models to entire mire areas was successful. The upscaled flark area coverage closely resembled the visual interpretation of the aerial orthoimagery. This suggests the model's efficacy in capturing the typical central flark fen patterns in aapa mires (Haapalehto et al. 2014; Tahvanainen 2011). Moreover, areas with lower flark coverage in the central wet zone typically correspond to locations of dry strings (Granlund et al. 2022; Sallinen et al. 2023). However, it is important to note that the random forest method tends to produce conservative estimates for extreme values (Coulston et al. 2016), potentially leading to a slight underestimation in flark-rich areas. Future studies could be conducted to compare different modelling algorithms for flark area prediction.

Talvitie, Räsänen, and Silvan (2023) demonstrated the feasibility of monitoring seasonal and multi-year variations in flark coverage using aerial and PlaneScope imagery. This was also demonstrated by Kolari et al. (2022) by utilizing individual images from 1988, 1997 and 2019. Given the availability of Landsat imagery since 1980s, our developed methodology of flark coverage predictions could be applied to assess the long-term changes at specific sites, which is essential for future monitoring needs and targets (Global Biodiversity Framework 2024). However, this would require appropriate training data, as multi-site models have shown some limitations. Talvitie, Räsänen, and Silvan (2023) used PlanetScope imagery for flark area classification, similar to our approach with UAV images. This suggest that PlanetScope could also provide multitemporal training data for models using coarser resolution imagery; however, PlanetScope is available only from 2016.

5. Conclusions

We tested three different optical satellite products for predicting aapa mire flark area coverage and investigated the effect of spatial and spectral resolution on the predictive capacity. We utilized UAV images to produce high spatial resolution flark area classifications and used them as training data for random forest regression. We predicted flark coverage separately for every site but also tested the model transferability between the sites. Our results indicate that all three tested satellite image sensors have a good accuracy in single-site flark area prediction, but PlanetScope and Sentinel-2 outperform Landsat, and the use of SWIR bands do not increase the model performance. Additionally, there are notable between-site differences in the results with single-site models being more accurate than models trained in multiple sites but transferred to an additional site. Our results also indicate that differences in modelling performance between early and late

summer imagery are small. The developed approach functions well in upscaling flark area beyond the area covered by UAV. Overall, the developed methodology shows promise for monitoring long-term changes in peatland hydrological and ecological conditions.

Acknowledgements

Disclosure statement

No potential conflict of interest was reported by the author(s).

Funding

ORCID

Aleksi Isoaho 🔟 http://orcid.org/0009-0008-0618-0889
Timo Kumpula 🔟 http://orcid.org/0000-0002-2716-7420

Data availability statement

The Sentinel-2 and Landsat 8–9 data used in this study is available at https://www.sentinel-hub.com/develop/api/. The PlanetScope data used in this study is available at https://www.planet.com/explorer/. All other data is available from the corresponding author upon reasonable request.

References

Bechtold, M., S. Schlaffer, B. Tiemeyer, and G. De Lannoy. 2018. "Inferring Water Table Depth Dynamics from ENVISAT-ASAR C-Band Backscatter Over a Range of Peatlands from Deeply-Drained to Natural Conditions." *Remote Sensing* 10 (4): 536. https://doi.org/10.3390/rs10040536.

Belgiu, M., and L. Drăguț. 2016. "Random Forest in Remote Sensing: A Review of Applications and Future Directions." *ISPRS Journal of Photogrammetry and Remote Sensing* 114 (April): 24–31. https://doi.org/10.1016/j.isprsjprs.2016.01.011.

Blaschke, T., G. J. Hay, M. Kelly, S. Lang, P. Hofmann, E. Addink, R. Queiroz Feitosa, et al. 2014. "Geographic Object-Based Image Analysis – Towards a New Paradigm." *ISPRS Journal of Photogrammetry and Remote Sensing* 87 (January): 180–191. https://doi.org/10.1016/j.isprsjprs.2013.09.014.

Bourgeau-Chavez, L. L., S. Endres, R. Powell, M. J. Battaglia, B. Benscoter, M. Turetsky, E. S. Kasischke, and E. Banda. 2017. "Mapping Boreal Peatland Ecosystem Types from Multitemporal Radar and Optical Satellite Imagery." *Canadian Journal of Forest Research* 47 (4): 545–559. https://doi.org/10.1139/cjfr-2016-0192.

Breiman, L. 2001. "Random Forests." *Machine Learning* 45 (1): 5–32. https://doi.org/10.1023/A:1010933404324.

Burdun, I., M. Bechtold, M. Aurela, G. De Lannoy, A. R. Desai, E. Humphreys, S. Kareksela, et al. 2023. "Hidden Becomes Clear: Optical Remote Sensing of Vegetation Reveals Water Table Dynamics in Northern Peatlands." *Remote Sensing of Environment* 296 (October): 113736. https://doi.org/10.1016/j.rse.2023.113736.

Burdun, I., M. Bechtold, V. Sagris, A. Lohila, E. Humphreys, A. R. Desai, M. B. Nilsson, G. De Lannoy, and Ü. Mander. 2020. "Satellite Determination of Peatland Water Table Temporal Dynamics by Localizing Representative Pixels of a SWIR-Based Moisture Index." *Remote Sensing* 12 (18): 2936. https://doi.org/10.3390/rs12182936.

Cole, B., J. McMorrow, and M. Evans. 2014. "Spectral Monitoring of Moorland Plant Phenology to Identify a Temporal Window for Hyperspectral Remote Sensing of Peatland." *ISPRS Journal of Photogrammetry and Remote Sensing* 90 (April): 49–58. https://doi.org/10.1016/j.isprsjprs.2014.01.010.

Comaniciu, D., and P. Meer. 2002. "Mean Shift: A Robust Approach Toward Feature Space Analysis." *IEEE Transactions on Pattern Analysis and Machine Intelligence* 24 (5): 603–619. https://doi.org/10.1109/34.1000236.

Coulston, J. W., C. E. Blinn, V. A. Thomas, and R. H. Wynne. 2016. "Approximating Prediction Uncertainty for Random Forest Regression Models." *Photogrammetric Engineering & Remote Sensing* 82 (3): 189–197. https://doi.org/10.14358/PERS.82.3.189.

Czapiewski, S., and D. Szumińska. 2021. "An Overview of Remote Sensing Data Applications in Peatland Research Based on Works from the Period 2010–2021." *Land* 11 (1): 24. https://doi.org/10.3390/land11010024.

ESA. 2023. "Sentinel Hub EO Browser." https://apps.sentinel-hub.com/eo-browser/.

Feyisa, G. L., H. Meilby, R. Fensholt, and S. R. Proud. 2014. "Automated Water Extraction Index: A New Technique for Surface Water Mapping Using Landsat Imagery." *Remote Sensing of Environment* 140 (January): 23–35. https://doi.org/10.1016/j.rse.2013.08.029.

Frazier, A. E., and B. L. Hemingway. 2021. "A Technical Review of Planet Smallsat Data: Practical Considerations for Processing and Using PlanetScope Imagery." *Remote Sensing* 13 (19): 3930. https://doi.org/10.3390/rs13193930.

Global Biodiversity Framework. 2024. "2030 Targets (With Guidance Notes)." https://www.cbd.int/gbf/targets.

Granlund, L., V. Vesakoski, A. Sallinen, T. H. M. Kolari, F. Wolff, and T. Tahvanainen. 2022. "Recent Lateral Expansion of Sphagnum Bogs Over Central Fen Areas of Boreal Aapa Mire Complexes." *Ecosystems* 25 (7): 1455–1475. https://doi.org/10.1007/s10021-021-00726-5.

Haapalehto, T., J. S. Kotiaho, R. Matilainen, and T. Tahvanainen. 2014. "The Effects of Long-Term Drainage and Subsequent Restoration on Water Table Level and Pore Water Chemistry in Boreal Peatlands." *Journal of Hydrology* 519 (November): 1493–1505. https://doi.org/10.1016/j.jhydrol.2014.09.013.

Haapalehto, T., H. Vasander, S. Jauhiainen, T. Tahvanainen, and J. S. Kotiaho. 2011. "The Effects of Peatland Restoration on Water-Table Depth, Elemental Concentrations, and Vegetation: 10 Years of Changes." *Restoration Ecology* 19 (5): 587–598. https://doi.org/10.1111/j.1526-100X.2010.00704.x.

Harris, A., and R. G. Bryant. 2009. "A Multi-Scale Remote Sensing Approach for Monitoring Northern Peatland Hydrology: Present Possibilities and Future Challenges." *Journal of Environmental Management* 90 (7): 2178–2188. https://doi.org/10.1016/j.jenvman.2007.06.025.

Hautala, R. 2022. "Vesien Palauttiminen Aapasoille : Kuinka Kasvillisuusanalyysi Tukee Ennallistamistoimien Ekologisen Vaikuttavuuden Arviointia." Master's thesis, University of Helsinki. https://helda.helsinki.fi/items/77b424c2-2fe5-4c98-b99c-6b9bf9f453da.

Huete, A. 1988. "A Soil-Adjusted Vegetation Index (SAVI)." *Remote Sensing of Environment* 25 (3): 295–309. https://doi.org/10.1016/0034-4257(88)90106-X.

Huete, A., K. Didan, T. Miura, E. P. Rodriguez, X. Gao, and L. G. Ferreira. 2002. "Overview of the Radiometric and Biophysical Performance of the MODIS Vegetation Indices." *Remote Sensing of Environment* 83 (1–2): 195–213. https://doi.org/10.1016/S0034-4257(02)00096-2.

Ikkala, L., A.-K. Ronkanen, J. Ilmonen, M. Similä, S. Rehell, T. Kumpula, L. Päkkilä, B. Klöve, and H. Marttila. 2022. "Unmanned Aircraft System (UAS) Structure-From-Motion (SfM) for

Monitoring the Changed Flow Paths and Wetness in Minerotrophic Peatland Restoration." *Remote Sensing* 14 (13): 3169. https://doi.org/10.3390/rs14133169.

Isoaho, A., L. Ikkala, L. Päkkilä, H. Marttila, S. Kareksela, and A. Räsänen. 2024. "Multi-Sensor Satellite Imagery Reveals Spatiotemporal Changes in Peatland Water Table After Restoration." *Remote Sensing of Environment* 306 (May): 114144. https://doi.org/10.1016/j.rse.2024.114144.

Isoaho, A., L. Ikkala, H. Marttila, J. Hjort, T. Kumpula, P. Korpelainen, and A. Räsänen. 2023. "Spatial Water Table Level Modelling with Multi-Sensor Unmanned Aerial Vehicle Data in Boreal Aapa Mires." *Remote Sensing Applications: Society and Environment* 32:101059. September. https://doi.org/10.1016/j.rsase.2023.101059.

Juel, A., G. Brian Groom, J.-C. Svenning, and R. Ejrnæs. 2015. "Spatial Application of Random Forest Models for Fine-Scale Coastal Vegetation Classification Using Object Based Analysis of Aerial Orthophoto and DEM Data." *International Journal of Applied Earth Observation and Geoinformation* 42 (October): 106–114. https://doi.org/10.1016/j.jag.2015.05.008.

Jussila, T., R. K. Heikkinen, S. Anttila, K. Aapala, M. Kervinen, J. Aalto, and P. Vihervaara. 2023. "Quantifying Wetness Variability in Aapa Mires with Sentinel-2: Towards Improved Monitoring of an EU Priority Habitat." *Remote Sensing in Ecology and Conservation* 10 (2): 172–187. https://doi.org/10.1002/rse2.363.

Kalacska, M., J. Pablo Arroyo-Mora, R. J. Soffer, N. T. Roulet, T. R. Moore, E. Humphreys, G. Leblanc, O. Lucanus, and D. Inamdar. 2018. "Estimating Peatland Water Table Depth and Net Ecosystem Exchange: A Comparison Between Satellite and Airborne Imagery." *Remote Sensing* 10 (5): 687. https://doi.org/10.3390/rs10050687.

Klinke, R., H. Kuechly, A. Frick, M. Förster, T. Schmidt, A.-K. Holtgrave, B. Kleinschmit, D. Spengler, and C. Neumann. 2018. "Indicator-Based Soil Moisture Monitoring of Wetlands by Utilizing Sentinel and Landsat Remote Sensing Data." *PFG – Journal of Photogrammetry, Remote Sensing and Geoinformation Science* 86 (2): 71–84. https://doi.org/10.1007/s41064-018-0044-5.

Kolari, T. H. M., A. Sallinen, F. Wolff, T. Kumpula, K. Tolonen, and T. Tahvanainen. 2022. "Ongoing Fen–Bog Transition in a Boreal Aapa Mire Inferred from Repeated Field Sampling, Aerial Images, and Landsat Data." *Ecosystems* 25 (5): 1166–1188. https://doi.org/10.1007/s10021-021-00708-7.

Kolari, T. H. M., and T. Tahvanainen. 2023. "Inference of Future Bog Succession Trajectory from Spatial Chronosequence of Changing Aapa Mires." *Ecology and Evolution* 13 (4): e9988. https://doi.org/10.1002/ece3.9988.

Kuhn, M. 2008. "Building Predictive Models in *R* Using the **Caret** Package." *Journal of Statistical Software* 28 (5). https://doi.org/10.18637/jss.v028.i05.

Lefebvre, G., A. Davranche, L. Willm, J. Campagna, L. Redmond, C. Merle, A. Guelmami, and B. Poulin. 2019. "Introducing WIW for Detecting the Presence of Water in Wetlands with Landsat and Sentinel Satellites." *Remote Sensing* 11 (19): 2210. https://doi.org/10.3390/rs11192210.

Leifeld, J., and L. Menichetti. 2018. "The Underappreciated Potential of Peatlands in Global Climate Change Mitigation Strategies." *Nature Communications* 9 (1): 1071. https://doi.org/10.1038/s41467-018-03406-6.

Lendzioch, T., J. Langhammer, L. Vlček, and R. Minařík. 2021. "Mapping the Groundwater Level and Soil Moisture of a Montane Peat Bog Using UAV Monitoring and Machine Learning." *Remote Sensing* 13 (5): 907. https://doi.org/10.3390/rs13050907.

McFeeters, S. K. 1996. "The Use of the Normalized Difference Water Index (NDWI) in the Delineation of Open Water Features." *International Journal of Remote Sensing* 17 (7): 1425–1432. https://doi.org/10.1080/01431169608948714.

Meingast, K. M., M. J. Falkowski, E. S. Kane, L. R. Potvin, B. W. Benscoter, A. M. S. Smith, L. L. Bourgeau-Chavez, and M. Ellen Miller. 2014. "Spectral Detection of Near-Surface Moisture Content and Water-Table Position in Northern Peatland Ecosystems." *Remote Sensing of Environment* 152 (September): 536–546. https://doi.org/10.1016/j.rse.2014.07.014.

Menberu, M. W., T. Tahvanainen, H. Marttila, M. Irannezhad, A. Ronkanen, J. Penttinen, and B. Kløve. 2016. "Water-Table-Dependent Hydrological Changes Following Peatland Forestry Drainage and Restoration: Analysis of Restoration Success." *Water Resources Research* 52 (5): 3742–3760. https://doi.org/10.1002/2015WR018578.

National Land Survey of Finland. 2023. "NLS Orthophotos." https://www.maanmittauslaitos.fi/en/maps-and-spatial-data/datasets-and-interfaces/product-descriptions/orthophotos.

Ozesmi, S. L., and M. E. Bauer. 2002. "Satellite Remote Sensing of Wetlands." *Wetlands Ecology and Management* 10 (5): 381–402. https://doi.org/10.1023/A:1020908432489.

Page, S. E., and A. J. Baird. 2016. "Peatlands and Global Change: Response and Resilience." *Annual Review of Environment and Resources* 41 (1): 35–57. https://doi.org/10.1146/annurev-environ-110615-085520.

Pang, Y., A. Räsänen, T. Juselius-Rajamäki, M. Aurela, S. Juutinen, M. Väliranta, and T. Virtanen. 2023. "Upscaling Field-Measured Seasonal Ground Vegetation Patterns with Sentinel-2 Images in Boreal Ecosystems." *International Journal of Remote Sensing* 44 (14): 4239–4261. https://doi.org/10.1080/01431161.2023.2234093.

Planet Team. 2023. "Planet Application Program Interface: In Space for Life on Earth." https://api.planet.com/.

Poulin, B., A. Davranche, and G. Lefebvre. 2010. "Ecological Assessment of Phragmites Australis Wetlands Using Multi-Season SPOT-5 Scenes." *Remote Sensing of Environment* 114 (7): 1602–1609. https://doi.org/10.1016/j.rse.2010.02.014.

Probst, P., M. N. Wright, and A.-L. Boulesteix. 2019. "Hyperparameters and Tuning Strategies for Random Forest." *WIREs Data Mining and Knowledge Discovery* 9 (3): e1301. https://doi.org/10.1002/widm.1301.

Räsänen, A., A. Tolvanen, and S. Kareksela. 2022. "Monitoring Peatland Water Table Depth with Optical and Radar Satellite Imagery." *International Journal of Applied Earth Observation and Geoinformation* 112 (August): 102866. https://doi.org/10.1016/j.jag.2022.102866.

Räsänen, A., and T. Virtanen. 2019. "Data and Resolution Requirements in Mapping Vegetation in Spatially Heterogeneous Landscapes." *Remote Sensing of Environment* 230 (September): 111207. https://doi.org/10.1016/j.rse.2019.05.026.

Räsänen, A., J. Wagner, G. Hugelius, and T. Virtanen. 2021. "Aboveground Biomass Patterns Across Treeless Northern Landscapes." *International Journal of Remote Sensing* 42 (12): 4536–4561. https://doi.org/10.1080/01431161.2021.1897187.

Riihimäki, H., M. Luoto, and J. Heiskanen. 2019. "Estimating Fractional Cover of Tundra Vegetation at Multiple Scales Using Unmanned Aerial Systems and Optical Satellite Data." *Remote Sensing of Environment* 224 (April): 119–132. https://doi.org/10.1016/j.rse.2019.01.030.

Rodriguez-Galiano, V. F., B. Ghimire, J. Rogan, M. Chica-Olmo, and J. P. Rigol-Sanchez. 2012. "An Assessment of the Effectiveness of a Random Forest Classifier for Land-Cover Classification." *ISPRS Journal of Photogrammetry and Remote Sensing* 67 (January): 93–104. https://doi.org/10.1016/j.isprsjprs.2011.11.002.

Rouse, J. W., R. H. Haas, J. A. Schell, and D. W. Deering. 1974. "Monitoring Vegetation Systems in the Great Plains with ERTS." *NASA Special Publications* 351 (1): 309.

Sadeghi, M., E. Babaeian, M. Tuller, and S. B. Jones. 2017. "The Optical Trapezoid Model: A Novel Approach to Remote Sensing of Soil Moisture Applied to Sentinel-2 and Landsat-8 Observations." *Remote Sensing of Environment* 198 (September): 52–68. https://doi.org/10.1016/j.rse.2017.05.041.

Sadeghi, M., N. Mohamadzadeh, L. Liang, U. Bandara, M. M. Caldas, and T. Hatch. 2023. "A New Variant of the Optical Trapezoid Model (OPTRAM) for Remote Sensing of Soil Moisture and Water Bodies." *Science of Remote Sensing* 8 (December): 100105. https://doi.org/10.1016/j.srs.2023.100105.

Sallinen, A., J. Akanegbu, H. Marttila, and T. Tahvanainen. 2023. "Recent and Future Hydrological Trends of Aapa Mires Across the Boreal Climate Gradient." *Journal of Hydrology* 617 (February): 129022. https://doi.org/10.1016/j.jhydrol.2022.129022.

Sallinen, A., S. Tuominen, T. Kumpula, and T. Tahvanainen. 2019. "Undrained Peatland Areas Disturbed by Surrounding Drainage: A Large Scale GIS Analysis in Finland with a Special Focus on Aapa Mires." *Mires and Peat* 24 (December): 1–22. https://doi.org/10.19189/MaP.2018.AJB.391.

Seppä, H. 2002. "Mires of Finland: Regional and Local Controls of Vegetation, Landforms, and Long-Term Dynamics." *Fennia - International Journal of Geography* 180 (1–2): 43–60.

Sirin, A., M. Medvedeva, A. Maslov, and A. Vozbrannaya. 2018. "Assessing the Land and Vegetation Cover of Abandoned Fire Hazardous and Rewetted Peatlands: Comparing Different Multispectral Satellite Data." *Land* 7 (2): 71. https://doi.org/10.3390/land7020071.

Sripada, R. P., R. W. Heiniger, J. G. White, and A. D. Meijer. 2006. "Aerial Color Infrared Photography for Determining Early In-Season Nitrogen Requirements in Corn." *Agronomy Journal* 98 (4): 968–977. https://doi.org/10.2134/agronj2005.0200.

Steenvoorden, J., and J. Limpens. 2023. "Upscaling Peatland Mapping with Drone-Derived Imagery: Impact of Spatial Resolution and Vegetation Characteristics." *GIScience & Remote Sensing* 60 (1): 2267851. https://doi.org/10.1080/15481603.2023.2267851.

Strack, M., A. Magnus Keith, and B. Xu. 2014. "Growing Season Carbon Dioxide and Methane Exchange at a Restored Peatland on the Western Boreal Plain." *Ecological Engineering* 64 (March): 231–239. https://doi.org/10.1016/j.ecoleng.2013.12.013.

Taddeo, S., I. Dronova, and N. Depsky. 2019. "Spectral Vegetation Indices of Wetland Greenness: Responses to Vegetation Structure, Composition, and Spatial Distribution." *Remote Sensing of Environment* 234 (December): 111467. https://doi.org/10.1016/j.rse.2019.111467.

Tahvanainen, T. 2011. "Abrupt Ombrotrophication of a Boreal Aapa Mire Triggered by Hydrological Disturbance in the Catchment." *Journal of Ecology* 99 (2): 404–415. https://doi.org/10.1111/j.1365-2745.2010.01778.x.

Talvitie, P., A. Räsänen, and N. Silvan. 2023. "Changes in the Open Water Hollows in Häädetkeidas and Kauhaneva Mires During 1947–2017 Based on Remote Sensing." *Suo - Mires and Peat* 74 (1–2): 71–96.

United Nations Environment Programme. 2022. *Global Peatlands Assessment: The State of the World's Peatlands*. https://www.unep.org/resources/global-peatlands-assessment-2022 .

Urák, I., T. Hartel, R. Gallé, and A. Balog. 2017. "Worldwide Peatland Degradations and the Related Carbon Dioxide Emissions: The Importance of Policy Regulations." *Environmental Science & Policy* 69 (March): 57–64. https://doi.org/10.1016/j.envsci.2016.12.012.

USGS. 2023. "Landsat Missions." https://www.usgs.gov/landsat-missions.

Vetrivel, A., M. Gerke, N. Kerle, and G. Vosselman. 2015. "Identification of Damage in Buildings Based on Gaps in 3D Point Clouds from Very High Resolution Oblique Airborne Images." *ISPRS Journal of Photogrammetry and Remote Sensing* 105 (July): 61–78. https://doi.org/10.1016/j.isprsjprs.2015.03.016.

Wilson, E. H., and S. A. Sader. 2002. "Detection of Forest Harvest Type Using Multiple Dates of Landsat TM Imagery." *Remote Sensing of Environment* 80 (3): 385–396. https://doi.org/10.1016/S0034-4257(01)00318-2.

Wolff, F., T. H. M. Kolari, M. Villoslada, T. Tahvanainen, P. Korpelainen, P. A. P. Zamboni, and T. Kumpula. 2023. "RGB Vs. Multispectral Imagery: Mapping Aapa Mire Plant Communities with UAVs." *Ecological Indicators* 148 (April): 110140. https://doi.org/10.1016/j.ecolind.2023.110140.

Zhou, Y., J. Dong, X. Xiao, T. Xiao, Z. Yang, G. Zhao, Z. Zou, and Y. Qin. 2017. "Open Surface Water Mapping Algorithms: A Comparison of Water-Related Spectral Indices and Sensors." *Water* 9 (4): 256. https://doi.org/10.3390/w9040256.